Design and Optimization for Simulated Moving Bed: Varicol Approach

Joana Matos, Rui P.V. Faria, José M. Loureiro, Ana M. Ribeiro, Idelfonso B. R. Nogueira*

* Laboratory of Separation and Reaction Engineering, Associate Laboratory LSRE-LCM
Department of Chemical Engineering, Faculty of Engineering, University of Porto
Rua Dr. Roberto Frias, 4200-465, Porto, Portugal, (e-mail: idelfonso@fe.up.pt)

Abstract: Simulated Moving bed adsorption processes are characterized by their complex dynamic behavior. Due to this issue, as deeper are explored their design possibilities, more complexity is expected. One example of this is the Varicol configuration. In this operating mode, it is possible to use more than one configuration in two consecutive switches through an asynchronous switch, reducing the unit costs in comparison with standard configurations. This work presents a new strategy for the design and concomitant optimization of SMB devices considering a Varicol operating mode. The optimization will include both the operating conditions and the configuration of the device. The optimization results enable the design of a Varicol configuration for the separation of the bi-naphthol enantiomers which can also be generelazied for other systems. The results have shown that including the configuration in the optimization process allows to increase the productivity of the separation process by 15% while reducing the total unit size.

Keywords: Unit Design, Process Optimization, SMB, Varicol, TMB, PSO,

1. INTRODUCTION

The design of separation units is commonly done separately from the optimization of the operating conditions. In complex devices such as the Simulated Moving Bed (SMB), the configuration of the unit is intrinsically connected to the performance of the unit. Commonly, the approaches that are used to optimize the operating conditions of units are mainly based on sensitivity analysis. These methods do not enable the evaluation of all possible operating conditions simultaneously since they perform a discrete analysis. Methods of this type that have already been applied are, for example, the triangle theory and the separation volume concept (Azevedo and Rodrigues 1999). The development of a systematic strategy to optimize SMB units is a complex and crescent issue in the literature (Nogueira et al. 2019, Li et al. 2020, Lee et al. 2020). In this work, an optimization process that includes both the operating conditions and the configuration will be used to design a new SMB device. The SMB device uses a chromatographical principal and is constituted by a series of packed bed columns in which the inlet and outlet streams are synchronously switched, using valves, in the direction of the fluid flow. The SMB has two inlets: the feed, F, and the eluent, E, and two outlets: the extract, X, and the raffinate, R. The position of the inlet and outlet streams defines the four sections of an SMB: Section I, between the eluent and the extract streams; section II, between the extract and the feed streams; section III between the feed and the raffinate streams and section IV between the raffinate and the eluent streams. The number of columns per section is called the *SMB design*. At the switching time, t^*, the inlets and outlets change their position cyclically, as shown in Fig.1. The synchronic switch of the SMB valves simulates a countercurrent contact between the solid and the liquid phases (Rodrigues et al. 2015). If the switch is asynchronous, it is possible to use more than one configuration in two consecutive switches and we have the called *Varicol* (Ludemann-Hombourger et al, 2000, Rodrigus et al. 2015). The definition of an optimal Varicol condition is still an open issue in the literature. Therefore, one of the contributions of this work is to propose a systematized strategy to perform the optimization of an SMB unit considering the Varicol operating mode. In this work, the Particles Swarm Optimization (PSO) algorithm will be used to optimize the operating conditions of the SMB and the length of the sections, i.e., the number of columns per section, which will enable to design a Varicol configuration for the bi-naphthol enantiomers system separation. The PSO algorithm was developed by Eberhart and Kennedy (1995) and uses a family of particles that keeps track of its coordinates to optimize systems. The PSO algorithm was previously applied to SMB devices, showing promising results (Wu et al. 2006, Matos 2017, Matos et al. 2019, Nogueira et al. 2019). The SMB will be represented by its theoretical model, the True Moving Bed (TMB) model, to develop a methodology that offers a reduced computation effort since it is possible to simulate the process directly in the steady state. As in SMB, the TMB model aims the maximization of the mass transfer in chromatographic separation processes through the counter-current movement between the solid and the liquid phases. The TMB model is simpler since it is considered that the solid actually moves. The boundary conditions are then continuous which makes the TMB equations much simpler to use in process simulation since the liquid phase equation is the same for each section (Rodrigues et al., 2015). The TMB is also constituted by four sections: the solid and the eluent are regenerated in sections I and IV, respectively, and the separation is done in sections II and III. The TMB configuration, i.e., the sections length, is then of massive importance as it influences the separation capacity of the dispositive. The optimization of the configuration will then be done in terms of the length of each section. The optimization results will be then converted to the equivalence values in a SMB unit. These values then be used

to obtain SMB Varicol configuration and operating conditions, which will be applied in a SMB unit in order to validate the strategy.
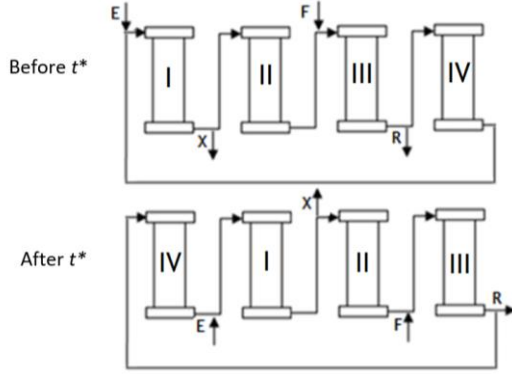
Fig. 1. SMB scheme.

2. MATHEMATICAL MODELS

2.1 Particles Swarm Optimization (PSO) Algorithm

The PSO algorithm was first developed by Eberhart and Kennedy (1995), and is based on a system of particles with dimension to $n_{it} \times n_p \times n_d$ in which n_{it} is the number of iterations, n_p is the number of particles and n_d is the number of parameters to be optimized. The algorithm here employed can be summarized in the following:

- Initialize the system by the calculation of

$$x_p = x_{min} + R(x_{max} - x_{min}) \qquad (1)$$
$$v = v_{max}(2R(1) - 1) \qquad (2)$$

where x_{min} and x_{max} are the minimum and maximum values for the optimization variables, R is a random number between 0 and 1 and v_{max} (Matos, 2017) is given by

$$v_{max} = \frac{x_{max} - x_{min}}{5} \qquad (3)$$

- Evaluate the objective function for each value of x_p;
- Select $x_{p_{best}}$ and $x_{g_{best}}$;
- Recalculate x_p and v, according to

$$x_p^{i+1} = x_p^i + v^{i+1} \qquad (4)$$
$$v^{i+1} = wv^i + c_1 R(1)\left(x_{p_{best}}^i - x_p^i\right) \\ + c_2 R(1)(x_{g_{best}}^i - x_p^i) \qquad (5)$$

where i is the iteration, $x_{p_{best}}$ is the best position of each particle, $x_{g_{best}}$ is the position of the best particle and w, c_1 and c_2 are parameters. w represents the "resistance of the particle to its movement" (Matos et al. 2019) and is determined by

$$w = w_0 + (w_f - w_0)\frac{i}{n_{it}} \qquad (6)$$

where w_0 is the inertia weight at the beginning of the search and w_f is the inertia weight at the end of the search (Shi and Eberhart, 1998). In this work, the values for the initial and final inertia weight were 0.9 and 0.4, respectively (Ratnaweera et al, 2004; Eberhart and Shi, 2001). c_1 and c_2 are respectively calculated at each iteration by (7).

$$c_1 = \frac{(0.5 - 2.5)i}{n_{it}} + 2.5 \qquad (7a)$$

$$c_2 = \frac{(2.5 - 0.5)i}{n_{it}} + 0.5 \qquad (7b)$$

- Loop until the maximum number of iterations.

In this work, the PSO algorithm and its variants, along with the objective functions that are used in this paper, were written in MATLAB.

2.2 Simulated Moving Bed (SMB)

The mathematical model used to describe the SMB unit is presented in Table 1.

Table 1. SMB Balances

Mass balance

Global Balances involving the feed, *f*, the raffinate, *r*, the eluent, *e*, and the extract, *x*

$$u_e + u_{IV}' = u_I'$$
$$u_I' = u_{II}' + u_x$$
$$u_{feed} + u_{II}' = u_{III}' \qquad (8)$$
$$u_{III}' = u_{IV}' + u_r$$

where u' are the fluid interstitial velocities of sections I, II, III and IV.

For compound *i* in column *k*, in the liquid phase

$$Dax_k'\frac{\partial^2 c_{ik}}{\partial z^2} - u_k'\frac{\partial c_{ik}}{\partial z} - \frac{1-\varepsilon}{\varepsilon}k_L(q_{ik}^* - q_{ik}) \\ = \frac{\partial c_{ik}}{\partial t} \qquad (9)$$

where z represents the axial position, t the integration time, Dax_k' is the axial dispersion, c_{ik} is the concentration, ε is the bulk porosity, k_L is the mass transfer coefficient (considering LDF model), q_{ik}^* is the concentration in the solid phase in equilibrium with the liquid phase and q_{ik} is the concentration in the solid phase.

For compound *i* in column *k*, in the solid phase

$$k_L(q_{ik}^* - q_{ik}) = \frac{dq_{ik}}{dt} \qquad (10)$$

Initial Conditions

$$c_{ik} = q_{ik} = 0, \text{at } t = 0 \qquad (11)$$

Boundary Conditions for column *k*

$$c_{ik} - \frac{Dax_k'}{u_{k'}}\frac{\partial c_{ik}}{\partial z} = c_{ik,0} \text{ , at } z = 0 \qquad (12)$$

$$\frac{dc_{ij}}{dz} = 0 \text{ , at } z = L_k'$$

for the eluent node, $c_{i(k+1),0} = c_{ik}\frac{u_{IV'}}{u_{I'}}$

for the feed node, $c_{i(k+1),0} = \frac{u_{II'}}{u_{III'}}c_{ik} + \frac{u_{feed}}{u_{III'}}c_i^{feed} \qquad (13)$

for the extract and raffinate nodes, $c_{i(k+1),0} = c_{ik}$

Parameters

$$Dax_k' = \frac{u_k'L_k'}{Pe} \qquad (14)$$

where L_k' is the length of column k and Pe is the Peclet number.

The SMB model was written in gPROMS and takes a few minutes to run. The Orthogonal Collocation in Finite Elements Method (OCFEM) with second order polynomials in a grid of 150 uniform intervals was used to perform the spatial

discretization of the PDEs which were then solved with DASOLV.

2.3 True Moving Bed (TMB) model

The mathematical model used to describe the TMB unit is presented in Table 2.

Table 2. TMB Balances

Mass balance

Global Balances involving the feed, *f*, the raffinate, *r*, the eluent, *e*, and the extract, *x*

$$u_e + u_{IV} = u_I$$
$$u_I = u_{II} + u_x$$
$$u_{feed} + u_{II} = u_{III} \qquad (15)$$
$$u_{III} = u_{IV} + u_r$$

where u are the fluid interstitial velocities of sections I, II, III and IV.

For compound *i* in section *j*, in the liquid phase

$$Dax_j \frac{d^2c_{ij}}{dz^2} - u_j \frac{dc_{ij}}{dz} - \frac{1-\varepsilon}{\varepsilon} k_L(q_{ij}^* - q_{ij}) = 0 \qquad (16)$$

where z represents the axial position, t the integration time, Dax_j is the axial dispersion coefficient, c_{ij} is the concentration, ε is the bulk porosity, k_L is the mass transfer coefficient (considering LDF model), q_{ij}^* is the concentration in the solid phase in equilibrium with the liquid phase and q_{ij} is the concentration in the solid phase.

For compound *i* in section *j*, in the solid phase

$$u_s \frac{dq_{ij}}{dz} + k_L(q_{ij}^* - q_{ij}) = 0 \qquad (17)$$

where u_s is the solid velocity.

Boundary Conditions for section *j* in the liquid phase

$$c_{ij} - \frac{Dax_j}{u_j}\frac{dc_{ij}}{dz} = c_{ij,0} \text{ , at } z=0 \qquad (18a)$$

$$\frac{dc_{ij}}{dz} = 0 \quad \text{, at } z = L_j$$

$$c_{iIV,L} = \frac{u_I}{u_{IV}} c_{iI,0}$$

$$c_{iI,L} = c_{iII,0} \qquad (18b)$$

$$c_{iII,L} = \frac{u_{III}}{u_{II}} c_{iIII,0} - \frac{u_{feed}}{u_{II}} c_i^{feed}$$

$$c_{iIII,L} = c_{iIV,0}$$

Boundary Conditions for section *j* in the solid phase

$$q_{iIv,L} = q_{iI,0}$$
$$q_{iI,L} = q_{iII,0} \qquad (19)$$
$$q_{iII,L} = q_{iIII,0}$$
$$q_{iIII,L} = q_{iIV,0}$$

Parameters

$$u = \frac{Q}{A\varepsilon} \qquad (20)$$

where Q is the volumetric flow-rate, A is the column section's area and ε is the porosity.

$$Dax_j = \frac{u_j L_j}{Pe} \qquad (21)$$

2.4 Equivalence between TMB and SMB

The equivalence between TMB and SMB in terms of velocities (by keeping the liquid velocity constant in relation to the solid velocity) or flow-rates, respectively can be expressed by

$$u_j' = u_j + u_s \qquad (22)$$

$$Q_j' = Q_j + \frac{1-\varepsilon}{\varepsilon} Q_s \qquad (23)$$

Here, Q_s and the switching time, t^*, are respectively given by

$$Q_s = \frac{1-\varepsilon}{t^*} V_c' \qquad (24)$$

$$t^* = \frac{L'}{u_s} \qquad (25)$$

where, L' is the length of the SMB column and V_c' is the volume of the SMB column (Rodrigues et al., 2015, Pais 1999).

3. OPTIMIZATION STRATEGY

In this work, the optimization of the TMB operating conditions is done using the volumetric flow-rates as decision variables which are the eluent, Q_e, the extract, Q_x, the recycle, Q_{IV}, the feed, Q_{feed} and the solid, Q_s, volumetric flow-rates. To optimize the configuration, the section lengths, L_I, L_{II} and L_{III} are added to the group of decision variables, **D**. The search dimension of the PSO algorithm is then equal to eight. The length of section IV, L_{Iv}, is determined using the total bed length, L, according to

$$L_{IV} = L - L_I - L_{II} - L_{III} \qquad (26)$$

The objective function used in this work is presented below, which is a constrained function written in terms of the productivity and the eluent consumption.

$$\min(Fobj) = EC - Prod + \omega \sum_{i=1}^{2} f_i^2 \qquad (27a)$$

$$\text{Subject to}$$
$$\mathbf{h(D)}=0 \qquad (27b)$$
$$EC(\mathbf{D}) \leq 0 \qquad (27c)$$
$$Prod(\mathbf{D}) \leq 0 \qquad (27d)$$
$$Pr \leq 0 \qquad (27e)$$
$$Px \leq 0 \qquad (27f)$$

in which **h** represents a path-type constraint vector associated with the set of governing equations. **h** is then a function of the decision variables, **D**, that were previously mentioned. In the objective function presented in Equation 27a, ω is the penalty coefficient and f_i is calculated by

$$f_i = P_i - P^{set} - |P_i - P^{set}| \qquad (28)$$

in which P_i is the extract or the raffinate purity and P^{set} is the desired purity. The raffinate and the extract purities are given by

$$P_r = \frac{C_A^r}{C_B^r + C_A^r} \qquad (29)$$

$$P_x = \frac{C_B^x}{C_B^x + C_A^x} \qquad (30)$$

The productivity, *Prod*, is given by

$$Prod = Prod_x + Prod_r \qquad (31)$$

$$Prod_x = \frac{Rec_x Q_{feed} C_B^{feed}}{(1-\varepsilon)V_c N_c} \quad (32)$$

$$Prod_r = \frac{Rec_r Q_{feed} C_A^{feed}}{(1-\varepsilon)V_c N_c} \quad (33)$$

where Rec_x and Rec_r are the extract and the raffinate recoveries, respectively, C_A^{feed} and C_B^{feed} are the feed concentration of A and B, respectively, ε is the bulk porosity, V_c is the TMB column volume and N_c is the number of columns (in the TMB case, N_c=1). The raffinate and extract recoveries are respectively determined by

$$Rec_r = \frac{Q_r C_A^r}{Q_{feed} C_A^{feed}} \quad (34)$$

$$Rec_x = \frac{Q_x C_B^x}{Q_{feed} C_B^{feed}} \quad (35)$$

where C_A^r and C_B^x are the mass concentrations of A and B in the raffinate and extract streams, respectively.

As a chiral separation is being performed, the eluent is also present in the feed. In this way, the eluent consumption, EC, is calculated by

$$EC = \frac{Q_e + Q_{feed}}{Q_{feed} \sum_{j=1}^{nc} c^{feed}} \quad (36)$$

in which nc is the number of components (Nogueira et al. 2016).

3.1 Convergence Criteria

To perform the optimizations, the maximum number of iterations used was equal to 2000. The convergence criteria is then evaluated in terms of the number of iterations that was needed to attain convergence, n_{it}^*.

For each iteration and each dimension of x_p, the criteria $\frac{\left|x_p^i - x_p^{n_{it}}\right|}{x_p^{n_{it}}} \times 100 \leq 1\%$ is applied. If the criteria $\leq 1\%$ is verified for all dimensions, n_{it}^*=i and convergence is assumed to have been attained (Matos et al. 2019).

4. RESULTS AND DISCUSSION

To perform the PSO optimizations of the TMB model reported in his work, the communication between gPROMS and MATLAB was done with gO:MATLAB, using a FPI (Foreign Process Interface) event. The simulations were run in a processor Intel® Core™ i5-2400 with a 3.10 GHz CPU. The RAM had an 8.00 GB capacity. The operating conditions are listed in Table 3.

Table 3. Operating Conditions

Total bed length, L (dm)	8
Column diameter (dm)	0.26
Porosity, ε	0.4
Feed concentration (g/L)	2.9
Mass transfer coefficient, k_L (min^{-1})	6
Peclet number, Pe	2000
Temperature, T (K)	303.15

To simulate the separation of the bi-naphthol enantiomers, a Pirkle type stationary phase, the 3,5-dinitrobenzoyl phenylglycine covalently bonded to silica gel (3,5-DNBPG-Silica) was used. The particles had a diameter of 25-40 μm and the eluent was a 72/28 heptane/isopropanol mixture. This system was studied by Pais (1999) who performed the experimental separation in a 12 column SMB (*Licosep* 12-26). The adsorption equilibrium isotherms were determined by the *Separex* group (Pais 1999): $q_A^* = \frac{2.69 c_A}{1+0.0336 c_A + 0.0466 c_B} + \frac{0.10 c_A}{1+c_A+3 c_B}$ and $q_B^* = \frac{3.73 c_B}{1+0.0336 c_A + 0.0466 c_B} + \frac{0.30 c_B}{1+c_A+3 c_B}$ in g/L.

4.1 PSO Optimization of TMB Model

The TMB will be optimized, considering the existence of all four sections, i.e., the length of each section is larger than $0.01L$. In this way, considering equal bounds for the sections that will be optimized, the maximum length for sections I, II and III is $L/3$. The optimization limits will then be between $0.01L$ and $L/3$. From this optimization, a SMB device with four sections will be designed. The path constraints of the decision variables are presented in Table 4. For the optimization, ten runs of the PSO method were performed which took approximately 24 hours. To illustrate the results, the run with the highest productivity, the average and the standard deviation (STD) are shown in Table 5.

Table 4. TMB optimization parameters.

	min	*max*
Q_E (mL/min)	0.01	200
Q_X (mL/min)	0.01	200
Q_{IV} (mL/min)	0.01	200
Q_{feed} (mL/min)	0.01	200
Q_s (mL/min)	0.01	200
L_I	0.01L	L/3
L_{II}	0.01L	L/3
L_{III}	0.01L	L/3
n_{it}	2000	
n_d	5	
n_p	50	
ω	4000	
w_0	0.9	
w_f	0.4	
$c1_0$	0.5	
$c1_f$	2.5	
$c2_0$	2.5	
$c2_f$	0.5	
P^{set}	0.97	

Table 5. TMB optimization results, *TMB-L*, (flow-rates in mL/min, productivity in g/L$_{ads}$/day, eluent consumption in dL/g and section's length in dm).

	TMB-L (best run)	TMB-L (average)	TMB-L (STD)	Matos et al. 2019	Wu et al. 2006
Q_E	80.8	78.4	2.3	27.4	22.1
Q_X	49.5	50.6	2.2	24.1	19.6

Q_{IV}	13.6	16.6	3.9	27.6	21.5
Q_{feed}	9.9	9.8	0.06	7	4.4
Q_s	17.5	17.3	0.35	12.1	9.0
L_I	1.8	1.7	0.18	-	-
L_{II}	2.8	2.8	0	-	-
L_{III}	2.8	2.8	0	-	-
P_r	0.97	0.97	0	0.97	0.99
P_x	0.97	0.97	0	0.97	0.98
$Prod$	299.5	297.3	2.1	212.3	144.0
EC	93.5	90.8	2.7	84.9	-
n_{it}^*	1801	1849	69	1888	-

Comparing Table 5 results with a representative run of the *optimization(ii)* results previously reported by Matos et al. (2019) for the same system it is visible that adding the sections length as an optimization variable leads to a better operating point since the productivity significantly increased (almost 30%). The eluent consumption slightly increased (5%) and the purities constraints were respected. The productivity of this work is about 50% higher than the results reported by Wu et al. (2006) for the optimization of the same system. As expected, this result shows that the length of the TMB sections plays a major role on the performance of the device, confirming that the design should be done in parallel with the optimization of the operating conditions (Matos 2017).

4.2 Varicol Design

As said in the Introduction, Varicol is a variant of the SMB with asynchronous shift of the inlet/outlet currents, i.e., the switching time is not the same for all the currents. To design a Varicol configuration, the optimization results of Section 4.1 were used. As shown in Table 3, the TMB configuration, i.e., the length of each section, obtained for *TMB-L* is 1.8-2.8-2.8-0.6. Normalizing in order to obtain an integer number of columns per section, the SMB configuration is 3-5-5-1. In this way, to use a regular SMB configuration, 14 columns were needed (Matos 2017). Here, Varicol will be used to reduce the number of columns, maintaining the total bed length; a seven column Varicol was, then, considered. To this purpose, the switching time was fractioned into two: on half of the time, the configuration was 1|3|2|1, and on the other half, it was 2|2|3|0. After the first half time, only the extract, X, and the raffinate, R, currents are switched; at the end of the second half, the eluent, E, and feed, F, currents are switched and the initial configuration is reset. Fig.2 shows schematically what happens to the section's length. The operating conditions to simulate the Varicol unit were obtained with (23) and (24): Q_E=80.8 mL/min, Q_X=49.5 mL/min, Q_{IV}=25.3 mL/min, Q_{feed}=9.9 mL/min and the switching time, t^*=2.18 min.

In Fig.2 it is visible that after the first switch, section IV disappears; in this case, the raffinate stream is collected before the dilution with the eluent stream (Ludemann-Hombourger et al, 2000).

The boundary condition and the node mass balance for section I are, respectively, given by

$$c_{iIII,L}\left(1 - \frac{u_r}{u_{III}}\right) = \frac{u_I}{u_{III}}c_{iI,0} \tag{37}$$

$$u_e + u_{III} - u_r = u_I \tag{38}$$
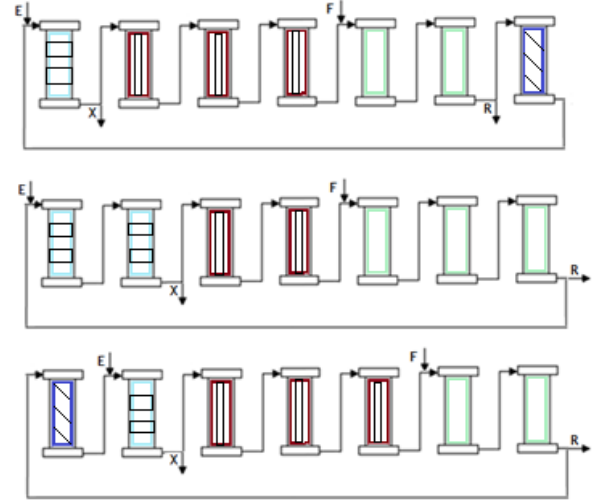
Fig. 2. Varicol configuration scheme (section I with horizontal lines, section II with vertical lines, section III in blank and section IV in diagonal lines).

The fact that there is a configuration change is also visible on the internal concentration profiles, shown in Fig.3. At the beginning of the switching time the internal concentration profile is represented by (1); at half of the switching time the configuration changes and the profile changes too (2); after the next half the initial configuration is reset as visible in (3).
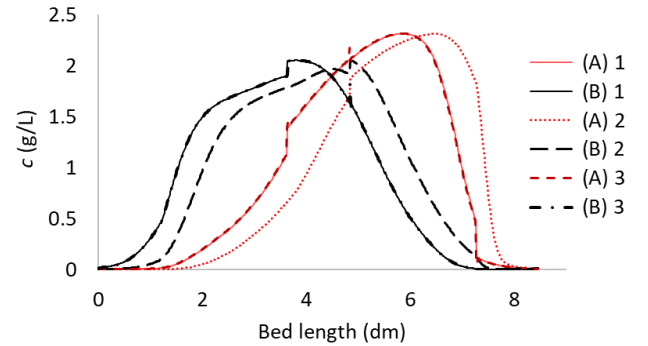
Fig. 3. Cyclic steady state (SMB) internal concentration profiles of the less (A) and the more (B) retained species for Varicol at the switching time (1 and 3); half of the switching time (2).

The productivity, the raffinate and the extract purities were, respectively, calculated by

$$Prod = \frac{Q_R \int_t^{t+N_c t^*} c_A^R \, dt}{(1-\varepsilon)V_c N_c t^*} + \frac{Q_X \int_t^{t+N_c t^*} c_B^X \, dt}{(1-\varepsilon)V_c N_c t^*} \tag{39}$$

$$P_R = \frac{\int_t^{t+N_c t^*} c_A^R \, dt}{\int_t^{t+N_c t^*} c_A^R \, dt + \int_t^{t+N_c t^*} c_B^R \, dt} \tag{40}$$

$$P_X = \frac{\int_t^{t+N_c t^*} c_B^X \, dt}{\int_t^{t+N_c t^*} c_A^X \, dt + \int_t^{t+N_c t^*} c_B^X \, dt} \tag{41}$$

This simulation results and the comparison with the TMB are shown in Table 6.

Table 6. Varicol results and comparison with TMB

	P_R	P_X	Prod (g/L$_{ads}$day)	EC (dL/g)
Varicol	0.96	0.96	281.2	93.4
TMB-L	0.97	0.97	299.5	93.5

Comparing with the TMB-L results (Table 5), Table 6 shows that the productivity decreased only 6% and the eluent consumption is nearly the same. In order to achieve purities of 0.97, changes in the operating conditions of the previous Varicol case were performed: Q_E and Q_{IV} increased 1% and 5%, respectively, and Q_{feed} was reduced 18% (Nogueira et al. 2016). Table 7 shows the comparison of this approach, Varicol-t, with the original Varicol and with the best SMB result reported by Matos et al. (2019).

Table 7. Varicol-t results and comparison with SMB

	P_R	P_X	Prod (g/L$_{ads}$day)	EC (dL/g)
Varicol-t	0.97	0.97	236.2	109.2
Varicol	0.96	0.96	281.2	93.4
SMB12 (Matos et al. 2019)	0.97	0.96	202.5	84.7

Comparing the optimized Varicol-t with previous results reported in the literature by Matos et al. (2019), Table 7 shows that the productivity increased by about 15%. Including the SMB design, i.e., the length of the sections, in the optimization not only enables to improve the separation performance in terms of productivity, but also it is possible to reduce the number of columns, which reduces the costs of the unit. If the usual SMB configuration was used, 14 columns would be needed as explained in section 4.2. With the Varicol configuration, the number of columns was reduced to 7, which is even smaller than the number of columns reported by Matos et al. (2019). In this work, the optimisation of the bi-haphthol enantiomers was used, but the design approach that was presented can be applied to other SMB separation cases.

5. CONCLUSIONS

A novel approach to design SMB Varicol processes was presented. Much higher productivity was obtained for the bi-naphthol system, comparing to the results previously published in the open literature: 30% higher than Matos et al. 2019 and 50% higher than Wu et al. 2006. The TMB results were used to define the Varicol configuration (i.e., number of columns per section). It was shown that defining the Varicol design from the optimization enables to increase the productivity of the SMB separation. In fact, the productivity increased 15% in relation to the result reported by Matos et al. (2019). Using the Varicol configuration, it is also possible to reduce the number of columns of the unit.

REFERENCES

Azevedo, D. C. S., Rodrigues, A. E. (1999). Design of a simulated moving bed in the presence of mass-transfer resistances. *AIChE Journal*, 45(5), 956–966.

Eberhart, R.C, Kennedy, J. (1995). A New Optimizer Using Particle Swarm Theory. *Proceedings of the Sixth International Symposium on Micro Machine and Human Science.*

Eberhart, R.C., Shi, Y. (2001). Particle Swarm Optimization: Developments, Applications and Resources. *Proceedings of the 2001 Congress on Evolutionary Computation*, 1, 81–86.

Lee, J.W., Kienle, A., Seidel-Morgenstern, A. (2020). On-line optimization of four-zone simulated moving bed chromatography using an Equilibrium-Dispersion Model: II. Experimental validation. *Chem. Eng, Sci.*, 115808-

Li, Y., Ding, Z., Wang, J., Xu, J., Yu, W., Ray, A. (2020). A comparison between simulated moving bed and sequential simulated moving bed system based on multi-objective optimization. *Chem. Eng, Sci.*, 115562.

Ludemann-Hombourger, O., Nicoud, R.M., Bailly M. (2000). The 'VARICOL' Process: A New Multicolumn Continuous Chromatographic Process. *Separation Science and Technology*, 35(12), 1829-1862.

Matos, J. (2017). *Particles Swarm Optimization for Chiral Separation by True Moving Bed Chromatography*. Master's Thesis. Faculdade de Engenharia da Universidade do Porto.

Matos, J., Faria, R.P.V., Nogueira, I.B.R., Loureiro, J.M., Ribeiro, A.M. (2019). Optimization strategies for chiral separation by true moving bed chromatography using Particles Swarm Optimization (PSO) and new Parallel PSO variant. *Computers and Chemical Engineering*, 123, 344-356.

Nogueira, I.B.R., Ribeiro, A.M., Rodrigues, A.E., Loureiro J.M. (2016). Dynamics of a True Moving Bed separation process: Effect of operating variables on performance indicators using orthogonalization method. *Computers and Chemical Engineering*, 86, 5-17.

Nogueira, I.B.R., Martins, A.F., Requião, R., Oliveira, A.R., Viena, V. Koivisto. H., Rodrigues, A.E., Loureiro, J.M., Ribeiro, A.M. (2019). Optimization of a True Moving Bed unit and determination of its feasible operating region using a novel Sliding Particle Swarm Optimization. *Computers and Chemical Engineering*, 135, 368-381.

Pais, L.S., Loureiro, J. M., Rodrigues, A.E. (1998). Modeling Strategies for Enantiomers Separation by SMB Chromatography. *AIChE Journal*, 44 (3), 561–69.

Pais, L.S. (1999). *Chiral Separation by Simulated Moving Bed Chromatography*. PhD Thesis. Faculdade de Engenharia da Universidade do Porto.

Rodrigues, A.E., Pereira, C., Minceva, M. Pais, L.S., Ribeiro, A. Ribeiro, A.M, Silva, M., Graça N., Santos, J.C. (2015). *Simulated Moving Bed Technology*. Edited by Fiona Gerghty. Joe Hayton.

Wu X., Jin, X., Xu, Z., Wang, S. (2006). Application of Particle Swarm Optimization in Process of Non-Linear Simulated Moving Bed Chromatographic Fractionation. *Control and Instruments in Chemical Industry*, 33, 5–9.